Research Article Vol. 6, No. 9 / September 2019 / Optica 1124

Low-threshold polariton lasing in a highly disordered conjugated polymer

Mengjie Wei,[1] Sai Kiran Rajendran,[1] Hamid Ohadi,[1] Laura Tropf,[1] Malte C. Gather,[1] Graham A. Turnbull,[1,2] and Ifor D. W. Samuel[1,3]

[1]Organic Semiconductor Centre, SUPA, School of Physics and Astronomy, University of St Andrews, St Andrews, KY16 9SS, UK
[2]e-mail: gat@st-andrews.ac.uk
[3]e-mail: idws@st-andrews.ac.uk

Received 18 March 2019; revised 1 June 2019; accepted 2 July 2019 (Doc. ID 362590); published 27 August 2019

Low-threshold, room-temperature polariton lasing is crucial for future application of polaritonic devices. Conjugated polymers are attractive candidates for room-temperature polariton lasers, due to their high exciton binding energy, very high oscillator strength, easy fabrication, and tunability. However, to date, polariton lasing has only been reported in one conjugated polymer, ladder-type MeLPPP, whose very rigid structure gives an atypically narrow excitonic linewidth. Here, we observe polariton lasing in a highly disordered prototypical conjugated polymer, poly(9,9-dioctylfluorene), thereby opening up the field of polymer materials for polaritonics. The long-range spatial coherence of the emission shows a maximum fringe visibility contrast of 72%. The observed polariton lasing threshold (27.7 μJ/cm^2, corresponding to an absorbed pump fluence of 19.1 μJ/cm^2) is an order of magnitude smaller than for the previous polymer polariton laser, potentially bringing electrical pumping of such devices a step closer.

https://doi.org/10.1364/OPTICA.6.001124

1. INTRODUCTION

Strong coupling between an exciton transition and a resonant cavity mode results in a bosonic quasi-particle, known as a cavity polariton [1–3]. The single-particle Hamiltonian for this system has in fact two new eigenstates—the lower and upper polariton branches (LPB and UPB). Due to the finite lifetime of polaritons, which is primarily caused by their photonic component, polaritons escape from the cavity and require pumping to maintain a steady population. Polaritons scatter along the LPB to lower energy states and can eventually accumulate in the common ground state. Stimulated scattering into a macroscopically occupied state leads to coherent light emission which is defined as polariton lasing [4–6]. Unlike conventional photon lasers, population inversion is not necessary for polariton lasing [7], which can lead to significantly lower thresholds [8].

Polariton lasing was first explored in inorganic semiconductor microcavities, where polariton condensation was observed [2,4,9,10]. Owing to the low binding energy of Wannier-Mott excitons in typical inorganic semiconductors, polariton lasing has been mainly demonstrated at cryogenic temperatures, with only a few exceptions at room temperature in ZnO [11,12], GaN [8,13–15], and perovskite nanoplatelets [16]. In comparison, organic semiconductors have high exciton binding energy and high oscillator strength, which are helpful for demonstrating stable room-temperature polariton lasing [17], and can be designed to emit across the visible spectrum. To date, a few organic materials have been studied for polariton lasing in planar dielectric microcavities, including crystalline anthracene [18], 2,7-bis[9,9-di(4-methylphenyl)-fluoren-2-yl]-9,9-di(4-methylphenyl) fluorene [19], a ladder-type poly(p-phenylene) polymer [20], a fluorescent protein [21], and most recently a molecular dye [22].

Conjugated polymers are particularly interesting for optoelectronic applications because they combine favorable optoelectronic properties with simple deposition from solution. They have been successfully used for a range of optoelectronic devices, including organic light-emitting diodes [23], solar cells [24], and lasers [25]. However, only one conjugated polymer has so far been reported to support polariton lasing [20]. This used the very rigid ladder-type conjugated polymer, MeLPPP, which has an unusually narrow excitonic linewidth with spectrally resolved vibronic replicas. Here, we show that the inhomogeneously broadened excitonic transition of the widely used poly(9,9-dioctylfluorene) (PFO) can strongly couple to the photon mode in a planar microcavity composed of distributed Bragg reflectors (DBRs) and exhibit evidence for low-threshold polariton lasing at room temperature based on a systematic characterization of the system [26–28].

2. METHODS

A. Sample Fabrication

The PFO used in this work was purchased from American Dye Source, Inc (ADS129BE). It was dissolved in toluene at a

concentration of 16 mg/mL and stirred overnight at 60°C. To obtain amorphous films (i.e., exclude formation of β-phase), the solution was heated on a hot plate at 110°C for 3 mins immediately prior to spin-coating. The bare film was spin-coated onto fused silica substrates for absorption, photoluminescence (PL), PL quantum yield (PLQY), and refractive index measurements.

For fabrication of microcavities, 10.5 pairs of Ta_2O_5/SiO_2 with thicknesses of 46.5 nm and 69.7 nm were deposited by radiofrequency magnetron sputtering onto fused silica as the bottom DBR. The center of the cavity was a 135-nm-thick PFO film, sandwiched between two 10-nm-thick SiO_2 layers. The top DBR was composed of 6.5 pairs of Ta_2O_5/SiO_2 using the same layer thicknesses as the bottom DBR. The entire process of microcavity fabrication was completed in a glovebox filled with nitrogen.

B. Characterization

The thickness and refractive index of PFO films and the transmission of DBRs were measured with spectroscopic ellipsometry (J.A. Woollam Co., Inc. M-2000DI). The absorption and emission spectra of the bare PFO film were measured with a Cary 300 UV-Vis spectrophotometer and an Edinburgh Instruments FLS980 spectrometer, respectively. The absolute PLQY measurement was performed using an integrating sphere in a Hamamatsu Photonics C9920-02 system [29]. The angle-resolved reflectivity from 0° to 40° was measured using a Fourier imaging microscope illuminated by polarized light from a Xenon lamp with a linear sheet polarizer. The reflected light was collected by a microscope objective (with magnification of 40 × and numerical aperture of 0.65) and then was detected by an Andor Shamrock 500SR CCD spectrometer. Due to the limitation on spectral transmittance through the microscope objective, there is no valid data in the ultraviolet region (<400 nm). Reflection data at higher angles, from 40° to 74°, in a wide spectral range (190–1700 nm) were obtained using the ellipsometer while illuminating samples with p-polarized white light.

The power-dependent angle-resolved PL measurement was performed using the same Fourier imaging microscope described above but with the microcavity pumped non-resonantly from the substrate side close to normal incidence. The PL was resolved using a 1200 grooves/mm grating in both spectra and angle. Vertically polarized excitation light at 343 nm was provided by the third harmonic of a Light Conversion Pharos laser. The pulse duration was 200 fs with a repetition rate of 5 kHz. The laser beam was a circular Gaussian spot of 175 μm diameter. A 400 nm long-pass filter was placed in front of the spectrometer to block the residual transmitted excitation laser beam. The absorbed threshold of polariton lasing is estimated from the incident lasing threshold by considering the absorbance of the PFO film in a round trip of the cavity and the transmittance of bottom and top DBRs [Fig. 1(b)]. Real-space images of light emission from the microcavity were measured using the spectrometer CCD camera, by removing the Fourier transform lens in the setup, opening the entrance slit completely, and aligning the grating to reflect the zeroth order to the camera.

For the spatial coherence measurements, microcavities were excited by the same laser, but were incident through a UV transmitting 40× microscope objective with a numerical aperture of 0.60 in reflection geometry, reducing the pump beam size to

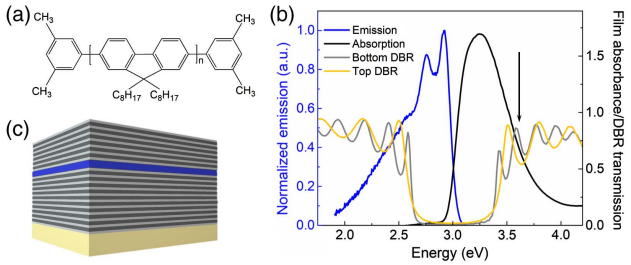

Fig. 1. (a) Chemical structure of PFO. (b) Absorption and emission spectra of a 135-nm-thick bare PFO film and transmission of the bottom and top DBRs at normal incidence. The black arrow indicates the excitation wavelength. (c) Schematic of the DBR microcavity.

24 μm in diameter. Emission from the microcavities was collimated by the objective and then split into two paths in a home-built Michelson interferometer with a non-polarizing cube beam-splitter. The Michelson interferometer included in a hollow retroreflector, used to invert the emission spot before interfering with the reference beam on the spectrometer CCD. A pair of color filters were used to block transmitted UV and residual infrared light from the excitation beam. All measurements were carried out at room temperature in air, but an external optical shutter was synchronized with the signal acquisition process of the spectrometer to reduce unnecessary photo-oxidation by the pump laser.

C. Fringe Visibility Contrast Fitting

The line profile of the interferogram was taken perpendicular to the fringes. The background signal was removed during the data acquisition process. The condition of measurements for images from separate interferometer arms and combined arms was kept the same. The line profile of the fringes was fitted by

$$LP_{\text{fringe}}(x) = LP_0(x)\left(1 + a\cos\left(\frac{2\pi}{d}x + \phi\right)\right), \quad (1)$$

where LP_0 is the sum of the emission intensity of line profiles taken from the same position in real-space images measured through each interferometer arm individually, $|a|$ is the fringe visibility contrast, d is the fringe spacing, and ϕ is a phase offset.

3. RESULTS AND DISCUSSION

PFO [see Fig. 1(a)] is a prototypical polymer in which the interchain bonding is highly sensitive to processing conditions, leading to different conformations with different photophysical properties [30–33]. The glassy amorphous form of the polymer was selected for the active layer of the polariton lasers reported here because of its homogeneous morphology within the film plane [31,33]. The absorption spectrum [Fig. 1(b)] exhibits an inhomogeneously broadened excitonic peak at 382 nm, while the emission spectrum shows partially resolved vibronic peaks at 424, 449, and 480 nm. The PFO thin films used in this study showed a high PLQY of ~50%.

The microcavities [Fig. 1(c)] were composed of a single layer of spin-coated PFO with 10-nm-thick SiO_2 underneath and above sandwiched between two dielectric mirrors (see also Section 2). The bottom and top DBRs were designed to have broad stopbands to cover the absorption and the main emission peaks, while having a high transmittivity to the excitation laser operating at a wavelength of 343 nm. The finesse and quality factor of the

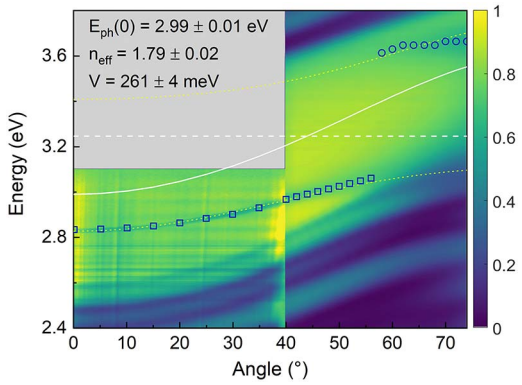

Fig. 2. Contour map of the *p*-polarized angle-resolved reflectivity for the 135-nm-thick microcavity. The experimental reflectivity minima are marked as open circles and squares in the map. Dotted yellow lines are matched results from a coupled oscillator model; the dashed and solid white lines are the uncoupled exciton and cavity photon, respectively. The fit parameters are given in the inset. Note: there is no valid data above 3.1 eV from 0 to 40° (gray region) because of the non-transparent microscope objective in ultraviolet region.

microcavities were calculated using the measured reflectivity of the mirrors to be ∼244, corresponding to an intra-cavity photon lifetime of 69 fs (see Supplement 1 Section 1).

The *p*-polarized angle-resolved reflectivity measured for a microcavity with a 135-nm-thick PFO film is shown in Fig. 2. To trace the full angular dispersion of the modes, the reflectivity was recorded from normal incidence up to 74° by a combination of Fourier imaging and ellipsometry as explained in Section 2. The positions of reflectivity minima identified on the individual spectra (see Supplement 1 Section 2, Fig. S1) are marked by open circles and squares in this map as a guide to the eye. The two dispersive features are identified as the LPB and UPB and indicate strong coupling between the excitonic transition at 3.246 eV (white dashed line) and the cavity resonance. Using a coupled oscillator model (see Supplement 1 Section 3), dispersive curves (yellow dotted lines) which match with the measured dispersion can be obtained. The coupled oscillator model also yields the position of the empty cavity mode (shown as solid white line in Fig. 2). We obtain a coupling strength (half Rabi splitting) of 261 meV for a cavity detuning of $\Delta = -254$ meV, corresponding to a 28% exciton fraction at the bottom of the LPB (Supplement 1 Fig. S2). The UPB is only visible at high angles due to absorption from uncoupled dark states in the disordered system, which have previously been seen in both inorganic and organic systems [19,34,35]. A transfer matrix model based on measured refractive index data (Supplement 1 Fig. S3) also shows good agreement with the measured dispersion (Supplement 1 Fig. S4).

The microcavity was then pumped non-resonantly at a wavelength of 343 nm by a pulsed laser with duration of 200 fs, repetition rate of 5 kHz, and beam diameter of ∼175 μm. The light emission was measured using a Fourier imaging setup, and the angular PL dispersion at different excitation densities is shown in Figs. 3(a)–3(c). At an incident pump fluence of 4.3 μJ/cm^2 ($0.2P_{th}$) [Fig. 3(a)], the observed emission overlaps well with the measured reflectivity dispersion of the lower polariton (dashed curve), indicating the emission originates from the LPB.

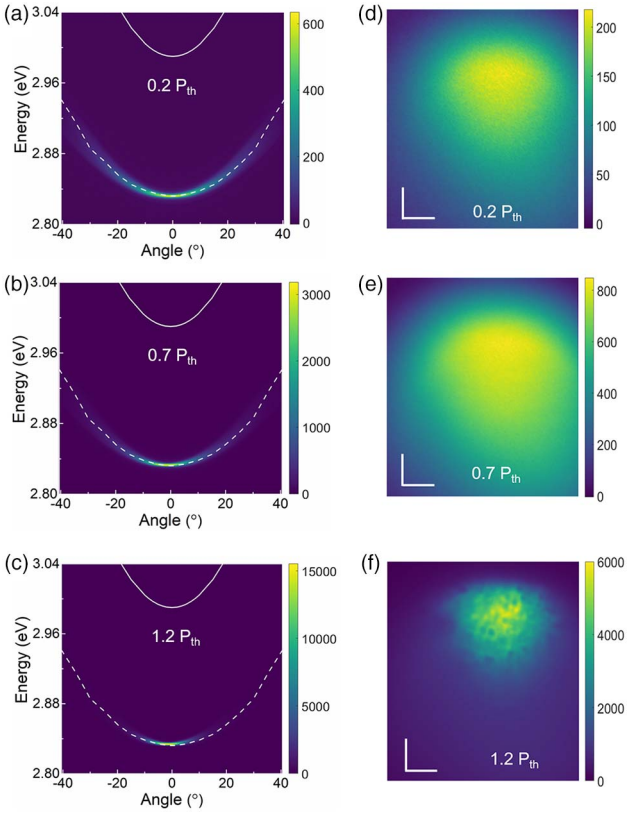

Fig. 3. Power-dependent angle-resolved PL spectra in Fourier-space and real-space images. The left panels (a)–(c) represent the lower polariton emission as a function of angle at incident pump fluence of 4.3 μJ/cm^2 ($0.2P_{th}$), 19.7 μJ/cm^2 ($0.7P_{th}$), and 33.8 μJ/cm^2 ($1.2P_{th}$). The dashed white lines indicate the measured lower polariton dispersion, and the solid white lines refer to the uncoupled cavity mode. The right panels (d)–(f) represent real-space images with corresponding excitation densities. The scale bars are 20 μm. The emission spot collapses to a smaller one when above threshold.

The emission is most intense at the in-plane wavevector $k_{//} = 0$ and decreases in intensity gradually towards high emission angles, which is caused by the reduction of photonic fraction along the LPB (Supplement 1 Fig. S2). On increasing the excitation energy to 19.7 μJ/cm^2 ($0.7P_{th}$), the emission narrows in both energy and angle [Fig. 3(b)]. When the incident pump fluence is increased to 33.8 μJ/cm^2 ($1.2P_{th}$), the lower polariton population occupies only energy states near the bottom of the branch [Fig. 3(c)]. We note that the dispersion of emission is well separated from the uncoupled cavity mode (white solid line), and the massive occupation of the lower polariton ground state signifies the emergence of polariton lasing [36]. The same plots but in logarithmic scale are shown in Supplement 1 Fig. S5.

We observe that the real-space emission area grows with increasing pump fluence below threshold, and collapses above threshold to a small spot of 52 μm diameter which is one-third of the diameter of the pumped region [Figs. 3(d)–3(f)]. This behavior follows a similar pattern to that reported in Ref. [19]. The collapse of the emission spot above threshold may be due to the reservoir-mediated instability of exciton-polariton condensates [37,38].

The power-dependence of the lower polariton emission at normal incidence ($k_{//} = 0$) is shown in Fig. 4. The emission peak

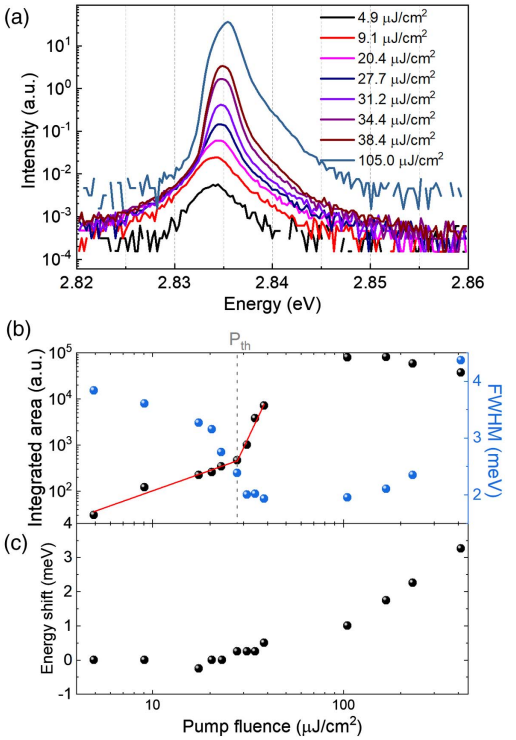

Fig. 4. (a) PL spectra at $k_{//} = 0$ extracted from the angle-resolved PL in Fourier space at different excitation energies. (b) The integrated area of emission spectrum at $k_{//} = 0$ and the full width at half maximum as functions of pump fluence. The transition from a linear regime to nonlinear regime defines the threshold at 27.7 μJ/cm². (c) Blue-shift of emission peak as a function of pump fluence.

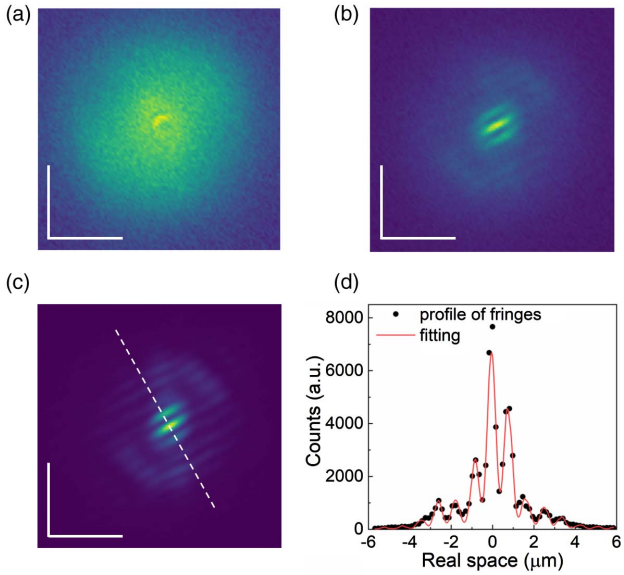

Fig. 5. Interferograms recorded in a Michelson interferometer for increasing pump fluence, (a) at 9.9 μJ/cm², (b) 18.3 μJ/cm², and (c) 27.5 μJ/cm². All scale bars are 5 μm. (d) The black solid circles are the intensity profile along the white dashed line in (c), and the red line is the fit (see Section 2).

is seen to narrow and continuously blue-shifts with increasing pump fluence comparing with the spectrum at the lowest pump fluence [Fig. 4(a)]. Figure 4(b) plots integrated areas from 3.04 eV to 2.77 eV as a function of pump fluence. The intensity of the lower polariton emission increases much faster above an incident pump threshold density of 27.7 μJ/cm², along with a reduction in linewidth from 3.8 meV to 1.9 meV, indicating the transition from a linear regime to a nonlinear regime [Fig. 4(b)]. On further increasing the pump fluence, the spectral linewidth broadens again, an effect that has also been described for other organic and inorganic polariton lasing microcavities [4,19] and that is likely to be due to self-interaction-induced decoherence and multimode lasing [39,40]. The occupancy of lower polaritons has also been extracted in Fig. S6 (Supplement 1) to show the thermalization of polaritons. Plotting the peak energy shift as a function of excitation fluence shows a blue-shift of the emission peak by around 3 meV at the highest excitation density [Fig. 4(c)]. This blue-shift may be attributed to repulsive self-interaction between polaritons [19–22,41], but we cannot rule out the contribution of other mechanisms.

Another important feature of polariton lasing is the emergence of long-range coherence. Long-range coherence can be obtained by interfering the real-space emission using a Michelson interferometer in which one arm is replaced by a retroreflector [4]. The power dependence of interferograms is shown in Fig. 5. When the pump fluence is below threshold at 9.9 μJ/cm² [Fig. 5(a)] no fringes are observed except for a small autocorrelation spot in the center, which shows that there is no long-range order below threshold. Near threshold (18.3 μJ/cm²) [Fig. 5(b)], the emission spot becomes more clearly defined in the center of the pump region, and interference fringes appear. When the pump intensity is increased further to 27.5 μJ/cm² [Fig. 5(c)], the emission spot matches the shape of pump beam and the fringes spread over the entire pump region along a distance over 10 μm (see also Supplement 1 Section 7, Fig. S7). We fitted the intensity profiles of the measured fringes with a cosine function multiplied by the sum of the emission intensity profiles from the two individual arms. This fit obtains a maximum fringe visibility contrast of 72% [Fig. 5(d)]. The spatial coherence can be further increased by expanding the pump beam size from 24 μm to 41 μm (see Supplement 1 Fig. S8).

In Fig. 6 we plot the emission peak intensity of the interferograms obtained at the same sample location in two sequential

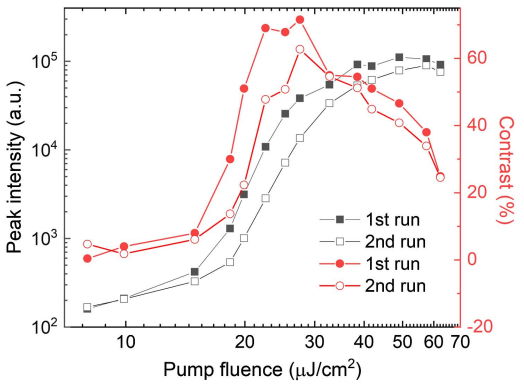

Fig. 6. Black solid and open squares, respectively, show the peak photoluminescence intensity of interferograms as a function of pump fluence in the first and second measurements. Red solid and open circles, respectively, show the fringe visibility for increasing pump fluence in the first and second measurements.

measurements as a function of the pump fluence. The peak intensity exhibits a nonlinear behavior above 16.3 $\mu J/cm^2$ (or 17.2 $\mu J/cm^2$ in the second run), similar to the polariton lasing threshold defined by the integrated intensity of spectrum at $k_{//} = 0$. The corresponding fringe visibility increases from a value of 8% (attributed to noise) to a maximum of 72% at $1.7P_{th}$. When the pump fluence is further increased in these two measurements, the peak intensity grows more gradually while the fringe contrast starts to decrease, indicating a decoherence process induced by polariton-polariton interactions rather than photobleaching effects.

4. CONCLUSION

We observe polariton lasing at room temperature from a microcavity containing a spin-coated PFO film. The excitonic transition of PFO strongly couples to the cavity mode as evident from the measured and calculated dispersion of the LPB and UPB. The nonlinear increase of emission intensity, blue-shift of emission, decrease of linewidth at $k_{//} = 0$, and the build-up of long-range coherence provides evidence for polariton lasing. Unlike photon lasing, the polariton emission is 164 meV red-detuned from the bare cavity mode. Our work shows that low-threshold room-temperature polariton lasing is possible in conjugated polymers with inhomogeneously broadened absorption. The observed polariton lasing threshold of 27.7 $\mu J/cm^2$, corresponding to an absorbed threshold of 19.1 $\mu J/cm^2$, is one order of magnitude lower than that reported for the ladder-type poly(p-phenylene) conjugated polymer. A reduction in threshold is a crucial step towards future realization of electrically pumped polariton devices for optoelectronics [14,42–44].

The research data supporting this publication can be accessed at [45].

Funding. China Scholarship Council; Engineering and Physical Sciences Research Council (EP/L015110/1, EP/M025330/1).

Acknowledgment. We are thankful to Dr. Jonathan Keeling, University of St Andrews, for useful discussions towards the interpretation of the results.

See Supplement 1 for supporting content.

REFERENCES

1. C. Weisbuch, M. Nishioka, A. Ishikawa, and Y. Arakawa, "Observation of the coupled exciton-photon mode splitting in a semiconductor quantum microcavity," Phys. Rev. Lett. **69**, 3314–3317 (1992).
2. H. Deng, J. Homan, A. J. S. Ser, H. Deng, G. Weihs, and C. Santori, "Condensation of semiconductor microcavity exciton polaritons," Science **298**, 199–202 (2002).
3. R. J. Holmes and S. R. Forrest, "Strong exciton-photon coupling in organic materials," Org. Electron. **8**, 77–93 (2007).
4. J. Kasprzak, M. Richard, S. Kundermann, A. Baas, P. Jeambrun, J. M. J. Keeling, F. M. Marchetti, M. H. Szymánska, R. André, J. L. Staehli, V. Savona, P. B. Littlewood, B. Deveaud, and L. S. Dang, "Bose–Einstein condensation of exciton polaritons," Nature **443**, 409–414 (2006).
5. R. Balili, V. Hartwell, D. Snoke, L. Pfeiffer, and K. West, "Bose–Einstein condensation of microcavity polaritons in a trap," Science **316**, 1007–1011 (2007).
6. B. Deveaud-Plédran, "On the condensation of polaritons," J. Opt. Soc. Am. B **29**, A138 (2012).
7. A. Imamoglu, R. J. Ram, S. Pau, and Y. Yamamoto, "Nonequilibrium condensates and lasers without inversion: Exciton-polariton lasers," Phys. Rev. A **53**, 4250–4253 (1996).
8. A. Das, J. Heo, M. Jankowski, W. Guo, L. Zhang, H. Deng, and P. Bhattacharya, "Room temperature ultralow threshold GaN nanowire polariton laser," Phys. Rev. Lett. **107**, 1–5 (2011).
9. L. S. Dang, D. Heger, R. André, F. Bœuf, and R. Romestain, "Stimulation of polariton photoluminescence in semiconductor microcavity," Phys. Rev. Lett. **81**, 3920–3923 (1998).
10. R. M. Stevenson, V. N. Astratov, M. S. Skolnick, D. M. Whittaker, M. Emam-Ismail, A. I. Tartakovskii, P. G. Savvidis, J. J. Baumberg, and J. S. Roberts, "Continuous wave observation of massive polariton redistribution by stimulated scattering in semiconductor microcavities," Phys. Rev. Lett. **85**, 3680–3683(2000).
11. T.-C. Lu, Y.-Y. Lai, Y.-P. Lan, S.-W. Huang, J.-R. Chen, Y.-C. Wu, W.-F. Hsieh, and H. Deng, "Room temperature polariton lasing vs. photon lasing in a ZnO-based hybrid microcavity," Opt. Express **20**, 5530 (2012).
12. A. Das, J. Heo, A. Bayraktaroglu, W. Guo, T.-K. Ng, J. Phillips, B. S. Ooi, and P. Bhattacharya, "Room temperature strong coupling effects from single ZnO nanowire microcavity," Opt. Express **20**, 11830 (2012).
13. S. Christopoulos, G. B. H. Von Högersthal, A. J. D. Grundy, P. G. Lagoudakis, A. V. Kavokin, J. J. Baumberg, G. Christmann, R. Butté, E. Feltin, J. F. Carlin, and N. Grandjean, "Room-temperature polariton lasing in semiconductor microcavities," Phys. Rev. Lett. **98**, 1–4 (2007).
14. P. Bhattacharya, T. Frost, S. Deshpande, M. Z. Baten, A. Hazari, and A. Das, "Room temperature electrically injected polariton laser," Phys. Rev. Lett. **112**, 29–31 (2014).
15. A. Bhattacharya, M. Z. Baten, I. Iorsh, T. Frost, A. Kavokin, and P. Bhattacharya, "Output polarization characteristics of a GaN microcavity diode polariton laser," Phys. Rev. B **94**, 035203 (2016).
16. R. Su, C. Diederichs, J. Wang, T. C. H. Liew, J. Zhao, S. Liu, W. Xu, Z. Chen, and Q. Xiong, "Room-temperature polariton lasing in all-inorganic perovskite nanoplatelets," Nano Lett. **17**, 3982–3988 (2017).
17. D. G. Lidzey, D. D. C. Bradley, M. S. Skolnick, T. Virgili, S. Walker, and D. M. Whittaker, "Strong exciton-photon coupling in an organic semiconductor microcavity," Nature **395**, 53–55 (1998).
18. S. Kéna-Cohen and S. R. Forrest, "Room-temperature polariton lasing in an organic single-crystal microcavity," Nat. Photonics **4**, 371–375 (2010).
19. K. S. Daskalakis, S. A. Maier, R. Murray, and S. Kéna-Cohen, "Nonlinear interactions in an organic polariton condensate," Nat. Mater. **13**, 271–278 (2014).
20. J. D. Plumhof, T. Stoeferle, L. Mai, U. Scherf, and R. Mahrt, "Roomtemperature Bose–Einstein condensation of cavity exciton–polaritons in a polymer," Nat. Mater. **13**, 247 (2014).
21. C. P. Dietrich, A. Steude, L. Tropf, M. Schubert, N. M. Kronenberg, K. Ostermann, S. Höfling, and M. C. Gather, "An exciton–polariton laser based on biologically produced fluorescent protein," Sci. Adv. **2**, e1600666 (2016).
22. T. Cookson, K. Georgiou, A. Zasedatelev, R. T. Grant, T. Virgili, M. Cavazzini, F. Galeotti, C. Clark, N. G. Berloff, D. G. Lidzey, and P. G. Lagoudakis, "A yellow polariton condensate in a dye filled microcavity," Adv. Opt. Mater. **5**, 1–6 (2017).
23. J. H. Burroughes, D. D. C. Bradley, A. R. Brown, R. N. Marks, K. Mackay, R. H. H. Friend, P. L. Burns, and A. B. Holmes, "Burroughes1990 Light-emitting diodes based on conjugated polymers.pdf," Nature **347**, 539–541 (1990).
24. N. Sariciftci, L. Smilowitz, A. J. Heeger, and F. Wudl, "Photoinduced electron transfer from a conducting polymer to buckminsterfullerene," Science **258**, 1474–1476 (1992).
25. N. Tessler, G. J. Denton, and R. H. Friend, "Lasing from conjugated polymer microcavities," Nature **382**, 695–697 (1996).
26. M. Richard, J. Kasprzak, R. André, R. Romestain, L. S. Dang, G. Malpuech, and A. Kavokin, "Experimental evidence for nonequilibrium Bose condensation of exciton polaritons," Phys. Rev. B **72**, 1–4 (2005).
27. J. Kasprzak, D. D. Solnyshkov, R. André, L. S. Dang, and G. Malpuech, "Formation of an exciton polariton condensate: Thermodynamic versus kinetic regimes," Phys. Rev. Lett. **101**, 3–6 (2008).
28. A. Rahimi-Iman, A. V. Chernenko, J. Fischer, S. Brodbeck, M. Amthor, C. Schneider, A. Forchel, S. Höfling, S. Reitzenstein, and M. Kamp, "Coherence signatures and density-dependent interaction in a dynamical excitonpolariton condensate," Phys. Rev. B **86**, 1–10 (2012).
29. N. C. Greenham, I. D. W. Samuel, G. R. Hayes, R. T. Phillips, Y. A. R. R. Kessener, S. C. Moratti, A. B. Holmes, and R. H. Friend, "Measurement

of absolute photoluminescence quantum efficiencies in conjugated polymers," Chem. Phys. Lett. **241**, 89–96 (1995).
30. P. E. Shaw, A. Ruseckas, J. Peet, G. C. Bazan, and I. D. W. Samuel, "Exciton - Exciton annihilation in mixed-phase polyfluorene films," Adv. Funct. Mater. **20**, 155–161 (2010).
31. A. K. Bansal, A. Ruseckas, P. E. Shaw, and I. D. W. Samuel, "Fluorescence quenchers in mixed phase polyfluorene films," J. Phys. Chem. C **114**, 17864–17867 (2010).
32. M. Grell, D. D. C. Bradley, G. Ungar, J. Hill, and K. S. Whitehead, "Interplay of physical structure and photophysics for a liquid crystalline polyfluorene," Macromolecules **32**, 5810–5817 (1999).
33. J. Peet, E. Brocker, Y. Xu, and G. C. Bazan, "Controlled β-phase formation in poly(9,9-di-n-octylfluorene) by processing with alkyl additives," Adv. Mater. **20**, 1882–1885 (2008).
34. R. Houdré, R. P. Stanley, and M. Ilegems, "Vacuum-field Rabi splitting in the presence of inhomogeneous broadening: Resolution of a homogeneous linewidth in an inhomogeneously broadened system," Phys. Rev. A **53**, 2711–2715 (1996).
35. J. A. Cwik, P. Kirton, S. De Liberato, and J. Keeling, "Excitonic spectral features in strongly coupled organic polaritons," Phys. Rev. A **93**, 1–12 (2016).
36. V. B. Timoffeev, "Bose condensation of exciton polaritons in microcavities," Semiconductors **46**, 843–860 (2012).
37. N. Bobrovska, M. Matuszewski, K. S. Daskalakis, S. A. Maier, and S. Kéna-Cohen, "Dynamical instability of a nonequilibrium exciton-polariton condensate," ACS Photon. **5**, 111–118 (2017).
38. T. C. H. Liew, O. A. Egorov, M. Matuszewski, O. Kyriienko, X. Ma, and E. A. Ostrovskaya, "Instability-induced formation and nonequilibrium dynamics of phase defects in polariton condensates," Phys. Rev. B **91**, 1–12 (2015).
39. S. Kim, B. Zhang, Z. Wang, J. Fischer, S. Brodbeck, M. Kamp, C. Schneider, S. Höfling, and H. Deng, "Coherent polariton laser," Phys. Rev. X **6**, 011026 (2016).
40. D. Porras and C. Tejedor, "Linewidth of a polariton laser: Theoretical analysis of self-interaction effects," Phys. Rev. B **67**, 1–4 (2003).
41. M. Vladimirova, S. Cronenberger, D. Scalbert, K. V. Kavokin, A. Miard, A. Lemaître, J. Bloch, D. Solnyshkov, G. Malpuech, and A. V. Kavokin, "Polaritonpolariton interaction constants in microcavities," Phys. Rev. B **82**, 1–9 (2010).
42. C. Schneider, A. Rahimi-Iman, N. Y. Kim, J. Fischer, I. G. Savenko, M. Amthor, M. Lermer, A. Wolf, L. Worschech, V. D. Kulakovskii, I. A. Shelykh, M. Kamp, S. Reitzenstein, A. Forchel, Y. Yamamoto, and S. Höfling, "An electrically pumped polariton laser," Nature **497**, 348–352 (2013).
43. P. Bhattacharya, B. Xiao, A. Das, S. Bhowmick, and J. Heo, "Solid state electrically injected exciton-polariton laser," Phys. Rev. Lett. **110**, 1–5 (2013).
44. A. Bhattacharya, M. Z. Baten, I. Iorsh, T. Frost, A. Kavokin, and P. Bhattacharya, "Room-temperature spin polariton diode laser," Phys. Rev. Lett. **119**, 1–6 (2017).
45. M. Wei, S. K. Rajendran, H. Ohadi, L. Tropf, M. C. Gather, G. A. Turnbull, and I. D. W. Samuel, Low threshold polariton lasing in a highly disordered conjugated polymer (dataset), University of St Andrews Research Portal, 2019, https://doi.org/10.17630/786775ad-012e-4890-a029-73cdabd762b3.